# Assembly Kinetics of $bc_1$ Complex Membrane Protein Investigated by Using a Continuous-Angle Laser Light Scattering Technique

**Kazuo Onuma,*,† Noriko Kanzaki,† and Tomomi Kubota‡**

*Institute for Human Science & Biomedical Engineering, National Institute of Advanced Industrial Science and Technology, Central 6, 1-1-1 Higashi, Tsukuba, Ibaraki 305-8566, Japan, and National Institute of Advanced Industrial Science and Technology, Laboratory of Gene Function Analysis, Institute of Molecular and Cell Biology, Central 2, 1-1-1 Umezono, Tsukuba, Ibaraki 305-8566, Japan*

*Received: April 16, 2003*

The assembly kinetics of a membrane protein, the $bc_1$ complex, was investigated using a newly developed continuous-angle laser light scattering technique. The apparent molecular weight, the radius of gyration, and the fractal dimension of aggregates in the aqueous solutions were calculated by simultaneously measuring the angular dependence on the scattering intensity with a time resolution of 1 s. It was found that the assembly of the $bc_1$ complex proceeded via increases in both the size and packing of the internal structure of the aggregates. This feature was qualitatively the same irrespective of whether zinc was present in the solutions. However, the fractal dimension in the final stage of assembly clearly showed a difference depending on the presence or absence of zinc in the solutions. The observed difference was consistent with the appearance of amorphous or crystalline phases. The assembly rate was controlled by the presence of zinc as well as by the concentration of PEG, the crystallizing reagent. Finally, the observed data were compared to those observed in the aggregation process of inorganic biological molecules, calcium phosphate.

## Introduction

Investigation of three-dimensional conformation and assembly of protein molecules in solutions is essential to determining the behavior of these molecules in vivo in order to understand the relationship between this behavior and fatal deceases and to develop better drugs and functional foods. Quasielastic light scattering is one technique widely used to clarify the structure of biological molecules in a solution. Static light scattering (SLS), one of the light scattering techniques, is useful because it can estimate the apparent molecular weight, the radius of gyration, and the fractal dimension of aggregates that gives us information on the internal structure of aggregates. However, the application of SLS to the investigation of assembly kinetics of proteins has been limited because this technique entails the measuring of angular dependence on scattering intensity to obtain the necessary data. This has been done by mechanically rotating a photomultiplier around the solution cell. Up to 10 min is needed to finish one cycle of measurement, making it impossible to use this technique to investigate fast reaction kinetics. Tsutsui overcame this problem by developing a continuous-angle laser light scattering (CALLS) instrument that used an ellipsoidal mirror and a high-speed CCD camera instead of the photomultiplier to collect the scattered lights.[1,2] In this study, we used this new technique for the aqueous solutions of the $bc_1$ complex membrane protein. Several kinds of globular proteins have been investigated by using the light scattering technique;[3−12] however, there has been little research on membrane proteins. In our previous dynamic light scattering (DLS) study,[13] we investigated the size distribution and intermolecular interactions of the $bc_1$ complex and found that these parameters were strongly affected by the presence of zinc, an important trace element in vivo. The previous DLS study focused on molecules in a steady state, and no assembly process was observed. In the present study, we clarify the assembly process of the $bc_1$ complex and investigate the role of zinc in this process by using CALLS. The data are compared to those obtained for a representative inorganic biological molecule, calcium phosphate, and the difference in the assembly processes of both materials is discussed.

## Experimental Section

**1. Set Up of CALLS.** Figure 1 illustrates the CALLS instrument we used. A 20 mW He−Ne laser was used as a light source. An ellipsoidal mirror made from an original ellipsoid (EM-29, Yamada Kogaku Kogyo Co., Ltd.) and a high-speed CCD camera (TE/CCD-512 TK, Princeton Instruments Inc.) were used to simultaneously correct the scattered light from a wide range of scattering angles at a high angular resolution. An example of scattered light on the pixels of the CCD camera (the white parts in the ellipsoid) is also shown in the figure. The collected scattered light was transferred to a computer by dynamic memory access transfer through A/D conversion by using the 16-bit AD board of the CCD controller. The theoretical angular resolution is defined by (measured angle range)/(number of CCD pixels), and it is calculated to be 0.3°. However, other factors such as the size of the aperture in front of the imaging lens had a significant effect on the resolution. When we take all possible factors into account, the maximum angular resolution is estimated to be 0.6°. We can obtain data for the angular dependence on scattering intensity for angles ranging from 10 to 170° simultaneously within a time interval of 1 s.

* To whom correspondence should be addressed. Phone: +81-29-861-4832. Fax: +81-29-861-6149. E-mail: k.onuma@aist.go.jp.
† National Institute of Advanced Industrial Science and Technology.
‡ Institute of Molecular and Cell Biology.

10.1021/jp030446c CCC: $25.00 
Published on Web 09/17/2003

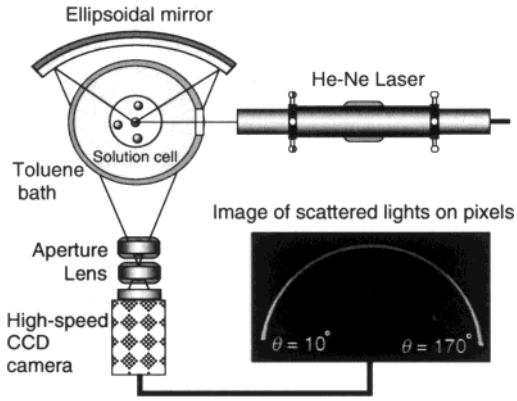


**Figure 1.** Schematic illustration of the continuous-angle laser light scattering instrument. The ellipsoid in the figure shows the raw image monitored on the CCD camera. The white parts indicate the scattered light.

**2. Composition of the $bc_1$ Complex Solution.** The molecular weight of the $bc_1$ complex is 240 kD, and the unit of a $bc_1$ complex molecule takes a dimer form, approximately 13 × 13 × 15.5 nm.[14−16] The preparation of the protein was reported elsewhere.[13,17] The aqueous solutions of the $bc_1$ complex in the present study contained a fixed concentration of $bc_1$ complex molecules at 50 $\mu$M and 36 mM of potassium phosphate at a pH of 8.0. Poly(ethylene glycol), PEG, (Merck, $M_w = 4000$) was added as a crystallization reagent, and the assembly process of $bc_1$ complex molecules depending on the concentration of PEG was monitored at 15 °C when 2 mM of zinc chloride were present and when zinc chloride was not present. Because the volume of the protein was limited, a tube cell with a 4.2 mm inner diameter designed for conventional neutron magnetic resonance measurement was used in the CALLS measurements.

**3. Composition of Calcium Phosphate Solution.** The aggregation of calcium phosphate and precipitation of hydroxyapatite ($Ca_{10}(PO_4)_6(OH)_2$) were observed using CALLS in the previous study.[18] However, the analysis of the change in the internal structure of the aggregates was insufficient. We reexamined the assembly process of calcium phosphate focusing on the change in the fractal dimension of the aggregates under a time resolution of 1s. The relationship between the scattered intensity and the whole range of scattering vectors was calculated to estimate the fractal dimension. This was not performed in the previous study. The calcium phosphate solution contained 2.5 mM $CaCl_2$ and 1 mM $K_2HPO_4 \cdot 3H_2O$ and it was buffered at pH = 7.4 by KOH. The measurements were performed at 25 °C.

## Principle of Data Analysis

**1. CALLS**. The apparent molecular weights, $M_w$, and the radii of gyration of scatterers, $\langle S \rangle$, are calculated using a Berry plot[19] as follows.

The Rayleigh ratio, $R$, at the scattering angle, $\theta$, is expressed using $M_w$, the concentration of aggregates or precipitates, $c$, the particle scattering function of scatterers, $P(\theta)$, and the optical constant, $K$, as

$$Kc/R(\theta)_{c=0} = 1/M_w P(\theta) \quad (1)$$

$$K = 4\pi^2 n^2 (dn/dc)^2 / N_A \lambda^4 \quad (2)$$

where $n$, $dn/dc$, $N_A$, and $\lambda$ denote the refractive index of the solvent, the specific refractive index increment, Avogadro's number, and the wavelength of the laser light, respectively.

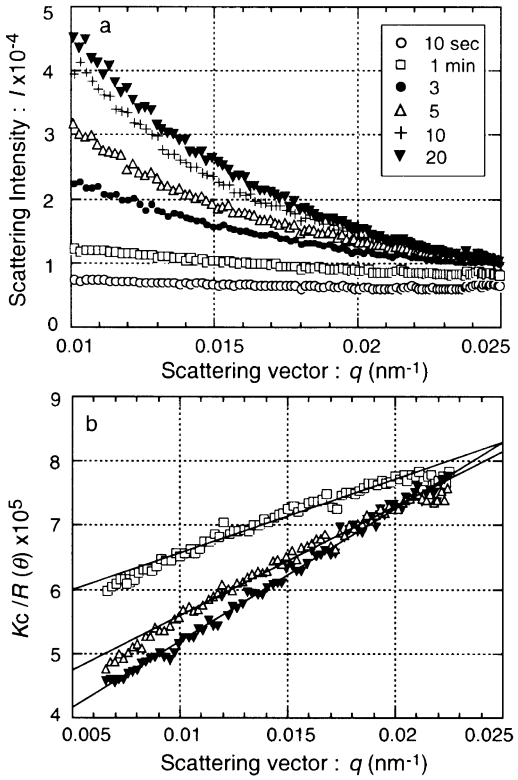


**Figure 2.** (a) Relationship between the scattering intensity and the scattering vector of the $bc_1$ complex solution without zinc depending on the time. The concentration of PEG is 6.8%. (b) Berry plots at $t$ = 1, 5, and 20 min. Symbols used are the same as those in part a.

Because $P(\theta) = 2(e^{-x} - 1 + x)/x^2$ and $x = q^2\langle S \rangle^2$, eq 1 can be expressed as

$$(Kc/R(\theta)_{c=0})^{1/2} = (1/M_w)^{1/2}(1 + q^2\langle S \rangle^2/6) \quad (3)$$

where $q$ ($=4\pi n \sin(\theta/2)/\lambda$) is the scattering vector.

**2. Fractal Dimension.** Over a certain limited range of length scale, the internal structure of aggregates shows a similar morphology independent of magnification. This fractal structure is characterized using the fractal dimension, $d$, which also indicates the compactness of the aggregates. The observed scattered intensity, $I(q)$, is related to $q$ and $d$ as follows:

$$I(q) = Cq^{-d} \quad (C: \text{ constant}) \quad (4)$$

This equation holds only when $1/\langle S \rangle < q < 1/r$, where $r$ is the radius of the essential unit forming the aggregates. When $q\langle S \rangle$ is close to unity, eq 4 does not hold anymore, and the following relationship should be used as reported by Bassi et al.:[20]

$$F(q\langle S \rangle) = \sin[(d-1)\arctan(q\langle S \rangle)]/(d-1)q\langle S \rangle(1 + q^2\langle S \rangle^2)^{(d-1)/2} \quad (5)$$

where $F(q\langle S \rangle)$ is the scale factor of the scatterers, which is proportional to the scattering intensity.

## Results

**1. Measurements of $M_w$, $\langle S \rangle$, and $d$ for the $bc_1$ Complex Solution.** Figure 2 shows the relationship between $I(q)$ and $q$ (Figure 2a) and the Berry plot (Figure 2b) for the solution without zinc. As described above, the measurements were performed within a time interval of 1 s, and the representative data are shown in the figure as a function of time. It can be seen from the figure that the intensity drastically increased

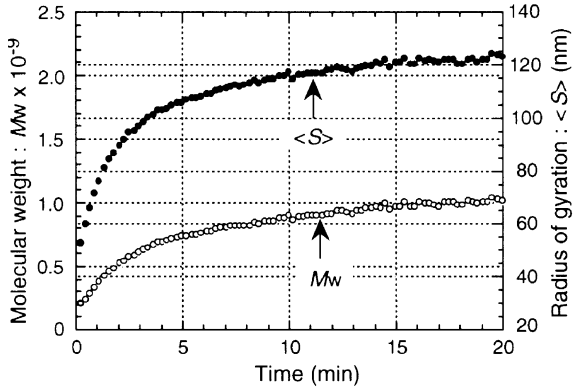


**Figure 3.** Change in $M_w$ (open circles) and $\langle S \rangle$ (closed circles) over time of the $bc_1$ complex solution without zinc. Note that $M_w$ values are apparent because the real d*n*/d*c* could not be measured in the present study.

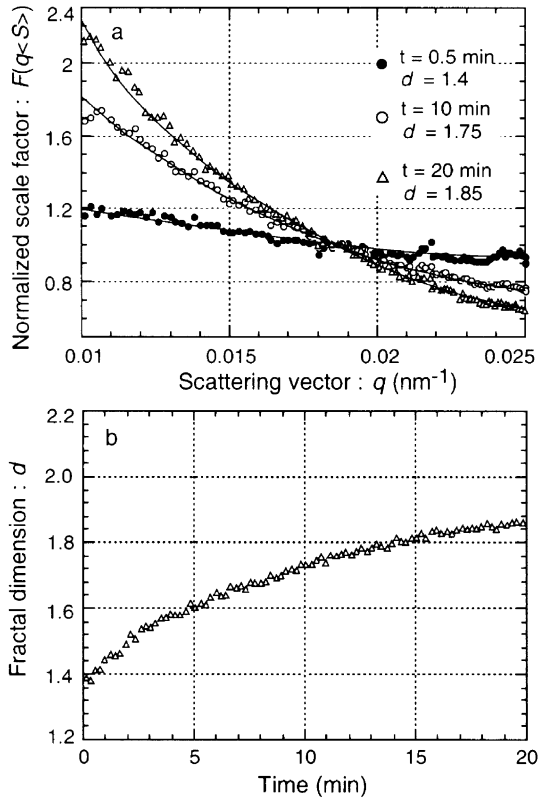


**Figure 4.** (a) Examination of fractal structure at different stages of $bc_1$ assembly without zinc. Note that the data for each stage were fitted by smooth curves without any discontinuous points. (b) The change in *d* over time.

within the first 10 min and then reached the maximum. The intensity shows a smooth decrease with the scattering vectors in each stage of assembly, which suggests a wide distribution of sizes of the scatterers. Using eqs 1−3, we calculated $M_w$ and $\langle S \rangle$ in relation to the time, and the results are presented in Figure 3. The calculated $M_w$ is an apparent value because the real d*n*/d*c* could not be measured owing to the small volume of protein. The data shown in the figure were reduced to $^1/_{15}$ of the raw data for ease of presentation. It should be noted that the temperature of the solution reached equilibrium 1 min after preparation; thus, the measurements started after this period. As seen in the figure, the $M_w$ increases fast in the initial 5 min, and in the next 15 min, it shows a gradual increase. The change in $\langle S \rangle$ coincides well with that in $M_w$ under this condition. The initial $\langle S \rangle$ of 50 nm drastically increases to 100 nm in the first

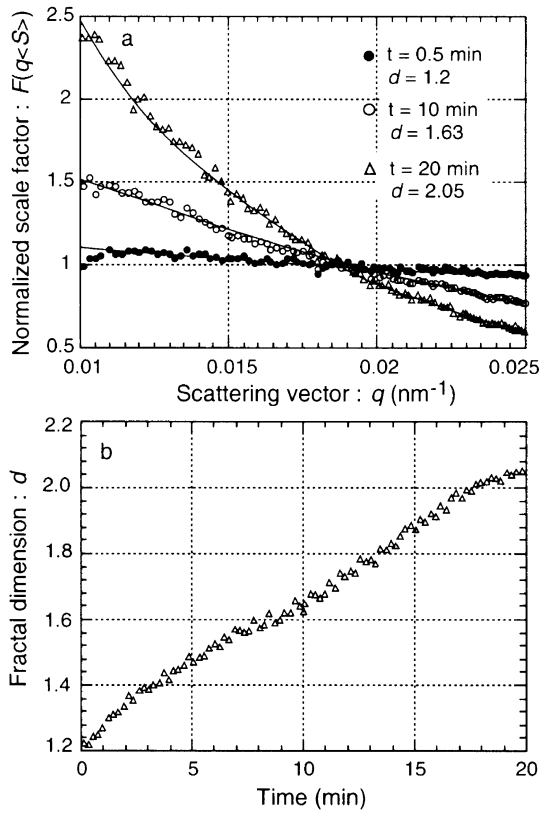


**Figure 5.** (a) *d* of $bc_1$ complex aggregates in the zinc-containing solution in three representative stages. *d* in the final stage is 2.05, larger than that observed in the zinc-free solution. (b) The change in *d* over time.

5 min and then slowly increases up to 125 nm at 20 min. In the final stage, the precipitation of the amorphous phase was observed. The concentration of PEG in this measurement was 6.8%. The value is a little smaller compared to that in our previous DLS study in which the aggregates were not observed until a PEG concentration of approximately 8.0% was reached. The reason for this is not clear, but a small amount of tris(hydroxymethyl)aminomethane buffer might have remained in the solution during the purification, which is known to decrease the critical concentration of PEG for precipitation.

Based on the $\langle S \rangle$ data in Figure 3, the fractal structure of the $bc_1$ complex in the assembly process without zinc was estimated. Because the range of *q* in this study is 0.01−0.025 $nm^{-1}$, and $\langle S \rangle$ is smaller than 130 nm, $q\langle S \rangle$ is 0.5−3.25. We, thus, used eq 5 to estimate *d*. When eq 4 is used, the *d* value is easily fixed from the log $I(q)$ − log *q* plot. However, if eq 5 is used, a least-squares method should be applied to calculate *d*. Figure 4a shows an example of the calculation of *d* in each stage of assembly. It is clear that the data can be fitted by smooth curves using appropriate *d* values, and there are no discontinuous points indicating that the fractal structure remains during assembly. The initial *d* was 1.4; it increased to 1.75 at 10 min, and finally took a value of 1.85. This calculation was performed in each stage of assembly, and the change in *d* with time is shown in Figure 4b. It can be seen that the *d* value increases especially in the early stage and then reaches the maximum. No discontinuous change in the *d* during the assembly was observed. This behavior is similar to that observed in the changes of $M_w$ and $\langle S \rangle$.

Figure 5 shows the calculation of *d* depending on the time when 2 mM zinc was added to the solution. Even when zinc was in the solution, the changes in $M_w$ and $\langle S \rangle$ were qualitatively

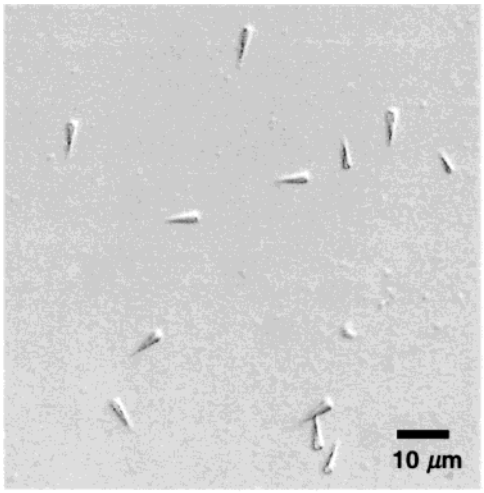


**Figure 6.** Single crystals of the $bc_1$ complex nucleated in the zinc-containing solution.

the same as in the absence of zinc. Both $M_w$ and $\langle S \rangle$ increased quickly in the first 5 min and then gradually reached the maximum, as did the data in Figure 4. *d*, however, took a slightly different value from that observed in the absence of zinc. As shown in Figure 5a, *d* was calculated as 1.2 at 0.5 min, and it then changed to 1.63 at 10 min and finally increased to 2.05, a value larger than the one obtained without zinc. The change in *d* with time is shown in Figure 5b. *d* quickly changed in the initial stage of assembly, and it continued to increase up to the final stage. In the final stage of assembly, we observed nucleation of the $bc_1$ complex single crystal with highly anisotropic morphology like that of a spear as shown in Figure 6.

We changed the concentration of PEG from 6.5 to 7% in the present study, but the features described above were the same both in the presence and in the absence of zinc.

**2. Assembly Rates in the Initial Stage Depending on Zinc and PEG Concentrations.** We estimated the respective changes in $\langle S \rangle$ over time at different concentrations of PEG when zinc was present and when it was not present. As shown in Figure 7, parts a and b, at a PEG concentration of 6.5%, the rates of increase in $\langle S \rangle$ were almost equal in both cases. At PEG concentrations of 6.8% and 7.0%, on the other hand, the rates were larger when zinc was present as compared to those when zinc was not present. The respective ratios of the assembly rates (the tangent line at time zero) when zinc was present and when it was not present were approximately 0.9 at 6.5% PEG and 1.5 both at 6.8% and 7.0% PEG.

**3. Measurements for Calcium Phosphate Solution.** We reported the preliminary results of using CALLS to measure in calcium phosphate solution in the previous study.[18] It was found that amorphous calcium phosphate was formed in the initial stage of assembly, but it transformed into hydroxyapatite crystals following its precipitation with time. We showed then that the $M_w$ greatly increased over time, whereas the $\langle S \rangle$ of the aggregates only showed a slight change with time from 500 to 650 nm. Because the internal structure of the amorphous phase was loose, it was suggested that the amorphous aggregates incorporated the molecules without increasing their size with time and then changed the internal structure to a compact form to reduce the total free energy. A rough estimation of *d* with time supported this idea, although it was calculated only for the representative stage of assembly and *q*. We, thus, reexamined the assembly process of amorphous calcium phosphate in the present study with a particular focus on whether the fractal structure indeed

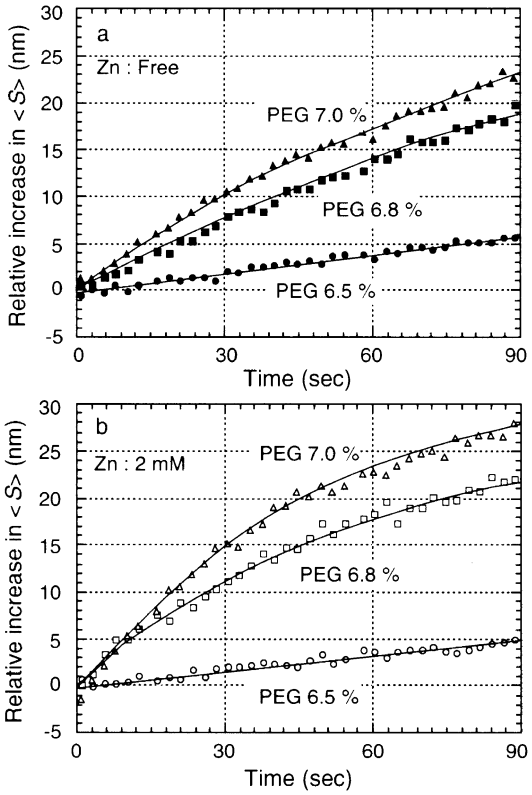


**Figure 7.** Increase in $\langle S \rangle$ over time as a function of the concentration of PEG in the zinc-free (a) and zinc-containing (b) solutions. At high concentrations of PEG, zinc contributes to the assembly of $bc_1$ complex.

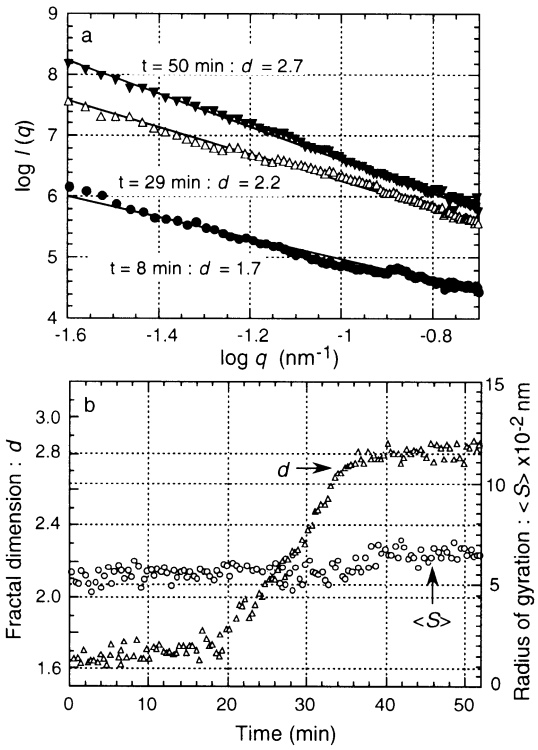


**Figure 8.** (a) Examination of fractal structure in different atages of assembly and the transformation of calcium phosphate. In all stages, the aggregates hold a fractal structure. (b) Change in *d* and $\langle S \rangle$ over time.

held during all of the stages. Figure 8a shows the log $I(q)$ vs log *q* plot at three different stages of assembly. Because $q\langle S \rangle$ is 6−15 and $qr < 0.0125$, taking the radius of the essential unit of amorphous calcium phosphate, $Ca_9(PO_4)_6$, 0.5 nm, into

account,[21−23] we can safely use eq 4 to calculate *d*. It can be seen in the figure that a linear relationship was found in all stages of assembly indicating that the assembly of amorphous calcium phosphate and the transformation into hydroxyapatite proceeded with holding the fractal structure. The change in *d* with time is shown in Figure 8b. It is clear that *d* changes in the three stages. In the first 20 min, *d* was almost constant, and in the next 20−35 min, it discontinuously increased, showing again a constant value of 2.7 after 35 min. In the figure, the change in $\langle S \rangle$ is also shown for reference.

## Discussion

Our observations of the $bc_1$ complex assembly are summarized below.

1. The assembly process proceeds via an increase in the value of $M_w$, $\langle S \rangle$, and *d*. This feature is fundamentally the same irrespective of whether zinc is present in or absent from the solutions.

2. Although the fractal structure holds in all of the stages of assembly, the *d* value continuously changes with time, and the final *d* is different depending on the presence or absence of zinc.

3. The assembly rate in the initial stage is controlled by both the PEG concentration and the presence of zinc.

The observations for calcium phosphate are summarized below.

4. The changes in the *d* value are classified into three stages depending on time.

The assembly process is usually thought to proceed via an accumulation of molecules, which leads to an increase in the apparent molecular weight and, hence, in the size of the aggregates. However, in the $bc_1$ complex, the internal structure also changes with time. The loose structure corresponding to a lower fractal dimension changes to a dense one corresponding to a higher fractal dimension. This indicates that the restructuring of the $bc_1$ molecules proceeds in an aggregate simultaneously with an increase in the total size of aggregates with time. It is interesting that both this process and the final product change with an addition of even a small amount of zinc. When zinc is absent, the fractal dimension in the final stage of assembly is 1.85. This value is larger than 1.75−1.8, assuming that the assembly proceeds in the diffusion-limited cluster−cluster aggregation regime (DLCA),[24] but it is smaller than 1.95−2.1, assuming a reaction-limited cluster−cluster aggregation (RLCA).[25] In DLCA, the assembly rate is controlled by the time during which the clusters collide with one another as a result of Brownian motion. On the other hand, in RLCA, the assembly rate is controlled by the probability that bonds may be forming between the neighboring clusters. When 2 mM zinc are added in the solution, the fractal dimension is 2.05 in the final stage. This value coincides well with that obtained assuming RLCA. Although the final fractal dimension is smaller than that expected from RLCA and an amorphous phase is formed in a zinc-free solution, this mechanism might be operating by taking into account the gradual change in the fractal dimension with time. The formation of an amorphous phase in the absence of zinc, and the appearance of a crystalline phase in the presence of zinc corresponds well to the difference in the fractal dimension in the final stage of assembly. Here, the question is why such a small amount of zinc (2mM) drastically affects the formation of the final product. The role of small ions on the assembly is usually attributed to the charge-screening effect that compensates for the counter charge on the protein surface following an increase in the attractive force between the molecules. However, this does not apply to the present case. As clarified in the previous DLS study, the intermolecular interactions between the $bc_1$ complex dimers were attractive in the absence of zinc and repulsive in the presence of zinc at a lower PEG concentration where no assembly takes place. The salt-bridging effect due to small ions is another possible explanation for the result. As reported for the formation of the insulin hexamer, certain cations specifically bind the protein forming a bridge between the molecules or aggregates. In this case, small amounts of zinc are enough to effectively form bonds, and the internal structure of the aggregates is ordered as compared to the case of simple aggregation without zinc. When another attractive force is acting on the molecules, salt bridging will proceed more effectively. This attractive force can be caused by the osmotic pressure of PEG (the so-called depletion effect) as discussed in several previous papers.[13,26,27] The faster assembly rate observed in the presence of zinc above the critical concentration of PEG indicates that the depletion effect and salt bridging cooperate in the assembly process. At a low concentration of PEG, there is no clear salt-bridging effect induced by the presence of zinc. At high PEG concentrations, on the other hand, zinc controls the assembly process, owing to the shorter distance between the aggregates caused by a strong attractive interaction by PEG.

The behavior of the fractal dimension with time seen in the calcium phosphate solution shows that the assembly of amorphous calcium phosphate in the initial stage (<20 min) proceeds with the fractal dimension being almost constant. This is contrary to the case that was observed in the formation of a $bc_1$ amorphous phase in the absence of zinc. In the final stage (> 35 min), this feature was also observed. The aggregates of hydroxyapatite crystals showed a constant fractal dimension value in contrast to the case of $bc_1$ assembly with a formation of a crystalline phase. Only in the middle stage (20−35 min) does the fractal dimension show a drastic change with time. This time-dependent change is analogous to that observed in $bc_1$; however, there is an essential difference between the two cases. In the calcium phosphate solution, the time-dependent change in the fractal dimension was observed during the transformation process, suggesting that there is a large energy gap between the amorphous and crystalline states. In contrast, in the $bc_1$, the difference in the formation kinetics of the amorphous and crystalline phases is very small as observed in the present study, indicating a small energy gap between the amorphous and crystalline phase. Only a small factor (the presence of zinc in the solution) controls the state of the final product. The difference in the assembly of small inorganic molecules and that of large protein molecules is attributed to the weak bonding between the molecules in the protein structure.

## Conclusion

The assembly process of the $bc_1$ complex increases both the size of the aggregates and the compactness of the internal structure. Zinc in the solution probably bridges the aggregates as a result of the strong depletion effect caused by PEG, following the appearance of a crystalline phase. However, the assembly kinetics of the formation of both the amorphous and crystalline phases was qualitatively the same. The internal structure gradually changed to amorphous or crystalline through the assembly of the molecules. This indicates that the energy difference between the amorphous and crystalline phases of the $bc_1$, a large molecular weight protein, is relatively small, which is in stark contrast to the case of small inorganic calcium phosphate molecules. The technique of continuous-angle laser light scattering with superior time and angular resolutions

enables us to monitor the dynamics of assembly of biological molecules. This new technique overcomes the drawback of conventional static light scattering

**Acknowledgment.** This study was supported by the Agency of Industrial Science and Technology (AIST).

## References and Notes

(1) Tsutsui, K.; Koya, K.; Kato, T. *Rev. Sci. Instrum*. **1998**, *69*, 3482.
(2) Tsutsui, K.; Kato, T. *Int. J. Polym. Anal. Charact*. **1999**, *5*, 257.
(3) Kadima, W.; McPherson, A.; Dunn, M. F.; Jurnak, F. A. *Biophys. J*. **1990**, *57*, 125.
(4) Georgalis, Y.; Zouni, A.; Saenger, W. *J. Cryst. Growth* **1992**, *118*, 360.
(5) Skouri, M.; Munch, J.-P.; Lorber, B.; Giege, R.; Candau, S. *J. Cryst. Growth* **1992**, *122*, 14.
(6) Kim, Y.-C.; Myerson, A. S. *J. Cryst. Growth* **1994**, *143*, 79.
(7) Eberstein, W.; Georgalis, Y.; Saenger, W. *J. Cryst. Growth* **1994**, *143*, 71.
(8) Muschol, M.; Rosenberger, F. *J. Chem. Phy.* **1995**, *103*, 10424.
(9) Boyer, M.; Roy, N.-O.; Jullien, M. *J. Cryst. Growth* **1996**, *167*, 212.
(10) Lafont, S.; Veesler, S.; Astier, J.-P.; Boistelle, R. *J. Cryst. Growth* **1997**, *173*, 132.
(11) Tanaka, S.; Ataka, M.; Onuma, K.; Astier, J.-P.; Veesler, S. *J. Cryst. Growth* **2002**, *237*, 289.
(12) Narayanan, J.; Liu, Y. Y. *Biophys. J*. **2003**, *84*, 523.
(13) Onuma, K.; T. Kubota, T.; Tanaka, S.; Kanzaki, N.; Ito, A.; Tsutsui, S. *J. Phys. Chem. B* **2002**, *106*, 4318.
(14) Akiba, K.; Toyoshima, T.; Matsunaga, T.; Kawamoto, M.; Kubota, T.; Fukuyama, K.; Namba, K.; Matsubara, H. *Nature Struct. Biol.* **1996**, *3*, 553.
(15) Xia, D.; Yu, C. A.; Kim, H.; Xia, J. Z.; Kachurin, A.; Zhang, L.; Yu, L.; Deisenhofer, J. *Science* **1997**, *277*, 64.
(16) Iwata, S.; Lee, J. W.; Okada, K.; Lee, J. K.; Iwata, M.; Ramaswamy, S.; Jap, B. K. *Science* **1998**, *281*, 64.
(17) Kubota, T.; Kawamoto, M.; Fukuyama, K.; Shinzawa-Itoh, K.; Yoshikawa, S.; Matsubara, H. *J. Mol. Biol*. **1991**, *221*, 379.
(18) Onuma, K.; Oyane, A.; Tsutsui, K.; Tanaka, K.; Treboux, G.; Kanzaki, N.; Ito, A. *J. Phys. Chem. B* **2000**, *104*, 10563.
(19) Berry, G. C. *J. Phys. Chem*. **1966**, *44*, 4550.
(20) Bassi, F. A.; Arcovito, G.; Spirito, M. De.; Morteente, A.; Martorana, G. E. *Biophy. J.* **1995**, *69*, 2720.
(21) Onuma, K.; Ito, A. *Chem. Mater*. **1998**, *10*, 3346.
(22) Treboux, G.; Layrolle, P.; Kanzaki, N.; Onuma, K.; Ito, A. *J. Phys. Chem. A* **2000**, *21*, 5111.
(23) Kanzaki, N.; Treboux, G.; Onuma, K.; Tsutsumi, S.; Ito, A. *Biomaterials*, **2001**, *21*, 2921.
(24) Martin, J. E.; Wilcoxon, J. P.; Scahefer, D.; Odinek, J. *Phys. Rev. A* **1990**, *41*, 4379.
(25) Lin, M.; Lindsay, H. M.; Weitz, D. A.; Ball, R. C.; Klein, R.; Meakin, P. *Phys. Rev. A* **1990**, *41*, 2005.
(26) Finet, S.; Tardieu, A. *J. Cryst. Growth* **2001**, *232*, 40.
(27) Tanaka, S.; Ataka, M.; *J. Chem. Phys*. **2002**, *117*, 3504.